ISSN: 2638-1974

International Journal of Petrochemistry and Research

Research Article

Open Access

A simple way to nickel based mesoporous carbons: Inexpensive nanocatalysts for the hydrogenolysis of sorbitol

Ying Yang*

State Key Laboratory of Heavy Oil Processing, China University of Petroleum, No.18, Fuxue Road,Changping District, Beijing 102249, China

Article Info

***Corresponding author:**
Dr. Ying Yang
State Key Laboratory of Heavy Oil Processing
China University of Petroleum
No.18, Fuxue Road, Changping District
Beijing 102249, China
Tel: +86-10-89734979
E-mail: catalyticscience@163.com

Received: September 29, 2018
Accepted: November 8, 2018
Published: November 15, 2018

Citation: Yang Y. A simple way to nickel based mesoporous carbons: Inexpensive nanocatalysts for the hydrogenolysis of sorbitol. *Int J Petrochem Res.* 2018; 2(3): 194-201.
doi: 10.18689/ijpr-1000135

Published by Madridge Publishers

Abstract

Non-precious nanocatalysts are of great importance both academically and industrially owing to their low cost and high performance in various reactions. Here in we report novel nickel based mesostructured carbon materials bearing homogeneously distributed nickel nanoparticles embedded inside the carbonaceous framework synthesized via fabrication of P123-directed chitosan-nickel superamolecular aggregates before pyrolysis. The mesostructure of support, and the dispersion, crystal and local structures of embedded nickel nanoparticles are fully examined by comprehensive characterization techniques, such as small-angle X-ray scattering, N_2 adsorption/desorption, TEM, high energy X-ray diffraction and X-ray absorption fine structure. All nickel based mesostructured carbons are active in the hydrogenolysis of sorbitol. Superior activity, total selectivity to 1,2-propylene glycol (1,2-PG) and ethylene glycol (EG), and recycling stability are shown when the molar ratio of Ni/CTS in the synthetic gel is 1/2 and the pyrolysis temperature is 550 °C, which can be ascribed to the controlled fabrication of uniform spherical nickel nanoparticles on the mesoporous carbon. This work may open new avenues for designing efficient metal catalysts by fabrication of surfactant-directed metal complex-containing superamolecular aggregates before pyrolysis.

Keywords: Self-assembly, Mesoporous carbon, Nickel, Sorbitol hydrogenolysis, 1,2-propylene glycol

Introduction

Conversion of biomass platform molecules into commodity chemicals has received extensive attention owing to the scarcity and high expense of fossil resources [1-4]. Among this line, the hydrogenolysis of renewable sorbitol to produce high value-added chemicals, like 1,2-propylene glycol (1,2-PG) and ethylene (EG), is a promising green process and is of great demand for producing polymers, resins, pharmaceuticals, cosmetics and functional fluids, etc [5]. Various heterogeneous nanocatalysts, such as Ni, Ru, Pd and Pt, have been designed for this process [6-9]. Non-precious nickel catalysts are superior to noble metal catalysts, since their usage can reduce cost fundamentally compared with using noble or doped noble metal catalysts. Correspondingly, various Ni-containing catalysts such as Ni-Kisseslguhr, Ni/SiO_2, Ni/Al_2O_3, Ni/TiO_2, Ni/ZrO_2, Ni/MgO, Ni-NaY and Ni-Ce/Al_2O_3, have been extensively synthesized and evaluated as catalysts for cellulose conversion, glucose hydrogenation, as well as sorbitol and glycerol hydrogenolysis owing to their inexpensive nature [6,8,10-13]. However, recent advances in synthesis of such catalysts focus on wetness

impregnation of nickel ions onto pre-formed metallic oxide support followed by reduction in H_2 atmosphere. This tedious post-synthetic method renders instable catalysts with unevenly dispersed Ni nanoparticles (Ni NPs) on the external surface or near pore mouths, even more worse, these oxide supports readily dissolves at elevated pH [6]. Despite continuous efforts, fabrication of homogeneously distributed Ni NPs onto a stable support *via* an economic synthetic procedure still remains a great challenge.

Carbon material is one of the best choices as the catalyst support due to its excellent chemical and hydrothermal stability, and large surface area for dispersing active components [14]. Particularly, mesoporous carbon (MC) materials offer great advantages over conventional activated carbons (AC) owing to their well-controlled mesopore structures, which are favorable to large molecule transportation [15]. However, mesoporous carbon (MC) supported metal catalysts are also prepared via traditional wetness impregnation before reduction, during which the MC must be elaborately fabricated by a tedious hard-templating approach. To replace such conventional "low efficient" preparations, pyrolysis of metal coordination polymers or metal organic frameworks under inert atmosphere is proved to be step-economic to *in situ* construct homogeneously dispersed metal nanoparticles inside the carbonaceous matrix, since the metal nanoparticles and carbonaceous matrix are synchronously fabricated during pyrolysis [16-17]. Whereas, the resulting carbonaceous frameworks are always microporous, disordered and lack of uniform pore size distributions, thus blocking mass transportation. To combine carbonaceous mesostructures with homogeneously dispersed metal nanoparticles, blending the thinking of mesopore formation via pyrolysis of surfactant-directed self-assemblies into pyrolysis of dispersion-controlled metal coordination polymers may be constructive.

To verify the hypothesis above, herein we try to synthesize a series of homogeneously distributed nickel based mesoporous carbons by pyrolysis of chitosan-nickel superamolecular aggregates, constructed by P123-directed self-assembly of 8-quinolinol modified chitosan (CTS-HQ) and nickel acetate with different Ni/CTS molar ratios under neutral conditions. Chitosan is preferentially chosen as carbon source and superior to the commonly used phenolic resin, polyamine, etc, since this naturally-occurring macromolecule is very abundant biodegradeble and biocompatible polysaccharide from alkaline deacetylation of chitin [18]. In this work, chitosan is pre-modified by 8-quinolinol to afford CTS-HQ, and to facilitate its binding and dispersion of metal ions more efficiently in sol-gel process, as well as its marriage with PEO moieties through H-bonding interaction well, rendering firmly fabricated superamolecular aggregates. The following pyrolysis under inert atmosphere at different temperatures is a unique "one stone, three birds" methodology to remove P123, carbonize CTS and reduce nickel ions by a single step. The resulting nickel catalysts are carefully characterized and screened as catalysts in the hydrogenolysis of sorbitol. The aim of this study is to develop a novel methodology for metal based mesoporous carbon design.

Experimental

Catalyst preparation

Nickel based mesoporous carbons were *in situ* prepared *via* pyrolysis of P123-directed chitosan-nickel superamolecular aggregates. First, CTS-HQ was facilely synthesized from 5-chloromethyl-8-quinolinol hydrochloride (1), involving only a two-step chemical transformation from 8-quinolinol (see Supporting Information and Figure S1-5).

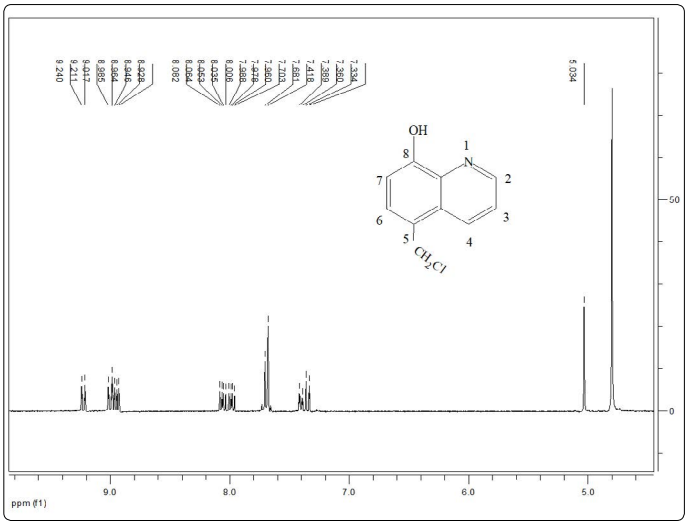

Figure S1. ^{1}H NMR spectrum of 1.

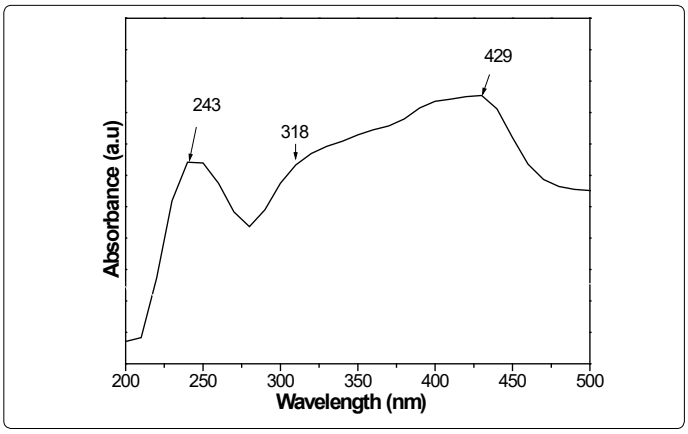

Figure S2. UV-vis spectrum of 1.

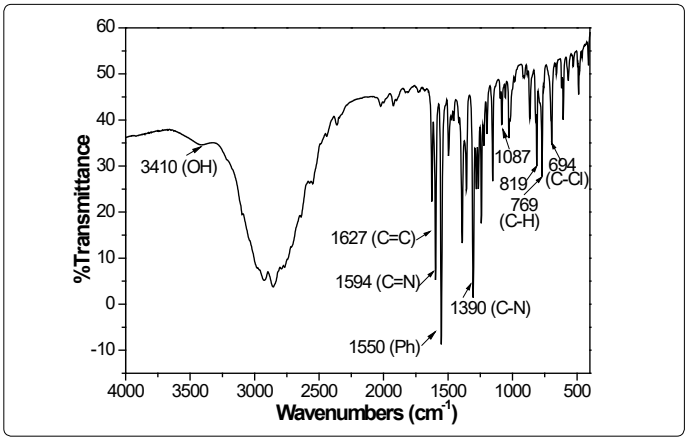

Figure S3. FT-IR spectrum of 1.

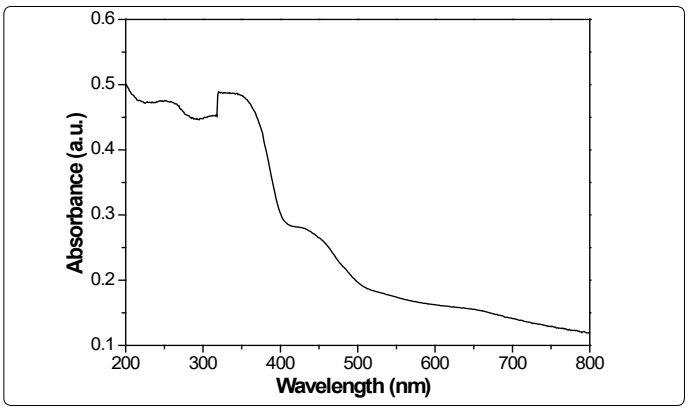

Figure S4. UV-vis spectrum of CTS-HQ.

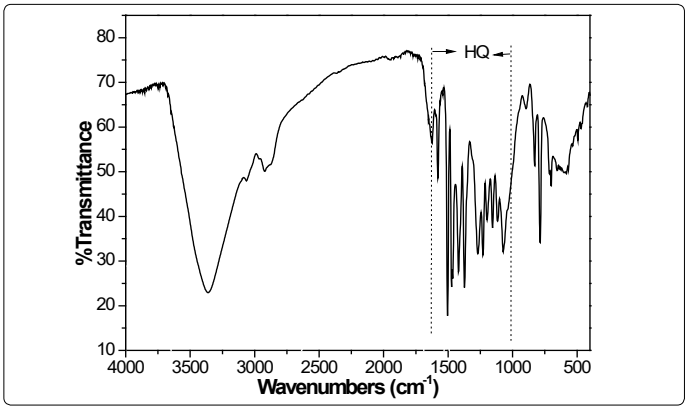

Figure S5. FT-IR spectrum of CTS-HQ.

CTS-HQ and $Ni(CH_3COO)_2{\cdot}4H_2O$ were respectively used as carbon source and metal precursor for the synthesis of precursor composite, Ni/CTS-P-x by P123-directed self-assembly (Scheme 1).

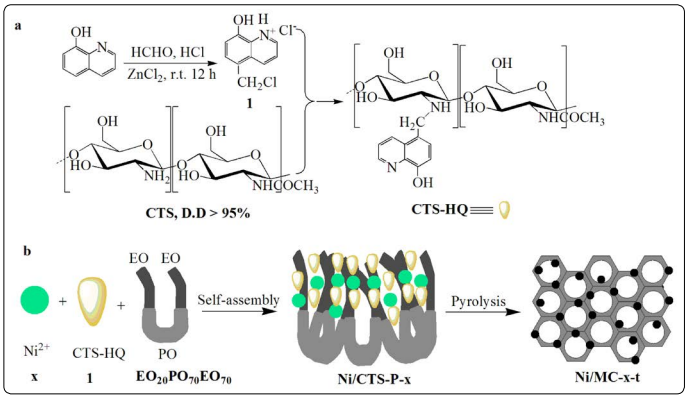

Scheme 1. Schematic illustrating of nickel based mesoporous carbon preparation. (a) Synthesis of 5-chloromethyl-8-quinolinol (1) and 8-quinolinol modified chitosan (CTS-HQ). (b) Fabrication of P123-directed precursor composite Ni/CTS-P-x before pyrolysis, yielding Ni/MC-x-t.

The molar ratio of the precursor gel in the preferred preparation is: 1 CTS-HQ: x $Ni(CH_3COO)_2{\cdot}4H_2O$: 0.017 P123: 66.5 H_2O: 19.6 EtOH, where x represents the Ni/CTS molar ratio, and was set to be 1/1, 1/2 and 1/4. In a typical synthesis, 2.0 g of P123 was dissolved in 48 ml of ethanol-water (50%, V/V) and stirred at 40 °C for 1 h, followed by addition of 2.32 g of CTS-HQ combined with certain amount of $Ni(CH_3COO)_2{\cdot}4H_2O$. The resulting mixture was stirred at 40 °C for 20 h and then transferred into a polypropylene bottle and reacted at 100 °C under static conditions for 48 h. The as-made product was washed, dried and pyrolyzed in a tubular furnace under N_2 atmosphere. The heating rate was 2 °C/min below 250 °C and 5 °C/min above 250 °C, and pyrolysis was carried out at 550, 750 and 950 °C for 2 h, respectively. The resulting solid was denoted as Ni/MC-x-t, where t represents the carbonization temperature.

Catalytic hydrogenolysis of sorbitol

The hydrogenolysis of sorbitol was carried out in a 100 ml stainless steel (SS) autoclave (Parr 4843) containing of 5.5 g of an aqueous solution of 9 wt% sorbitol, 0.5 g CaO and 0.05 g nickel based catalyst. The sealed autoclave was purged by flowing H_2 at room temperature. The autoclave was pressurized with H_2 to 6 MPa and was heated to 220 °C. Once the temperature was reached, the timing was started. During the reaction, the H_2 pressure in the autoclave kept constant due to the small amount of H_2 consumed. After being finished, the autoclave was cooled rapidly with cold water. Then a certain amount of 1,4-dioxane was added as the internal standard, and analyzed. Polyols were analyzed using a 6820 Gas Chromatography (GC) with a capillary column (AT™-AQUAWAX). Sorbitol was analyzed by HPLC (HPLC 1260, Agilent) equipped with an ELSD detector (ELSD-3000, Alltech) and a Prevail™ Carbohydrate ES HPLC Column at 25 °C. Redistilled water/acetonitrile (15/85) mixture was used as the mobile phase at a flow rate of 0.9 ml min^{-1}.

Results and discussion

Structural properties

High-energy X-ray diffraction (HE-XRD) was preferentially used to investigate the crystal structure of Ni species, due to its high flux and rapid analysis. figure 1 shows the HE-XRD patterns of various Ni-containing samples. As expected, different from nickel acetate, the representative Ni/CTS-P-1/2 shows no diffractions, corresponding to the coordination of Ni ions with CTS-HQ. Upon pyrolysis, all Ni/MC-x-t samples display XRD patterns of fcc-structured Ni (JCPDS file 04-0805) at (111), (200), (220), (311) and (222) diffractions, indicating the formation of Ni nanocrystallites [19]. However, the diffraction intensity decreases as the Ni content in the synthetic gel decreases (Figure 1c-e), and it is the same case when elevating pyrolysis temperature from 550 to 750 °C (Figure 1d,f,g), suggesting less Ni nanocrystals formed.

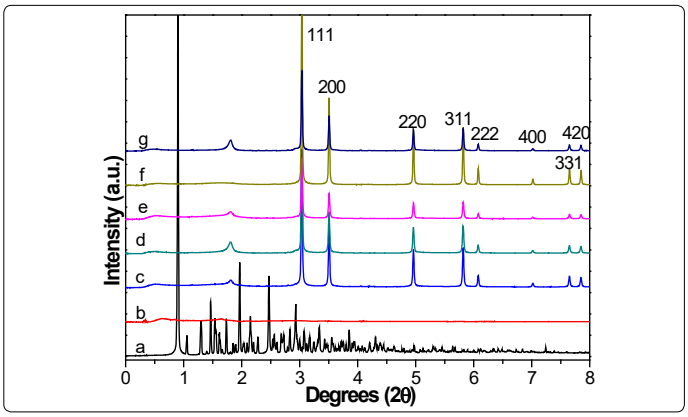

Figure 1. High-energy X-ray diffraction patterns of (a) $Ni(CH_3COO){\cdot}4H_2O$, (b) Ni/CTS-P-1/2, (c) Ni/MC-1/2-550, (d) Ni/MC-1/2-750, (e) Ni/MC-1/2-950, (f) Ni/MC-1/1-750 and (g) Ni/MC-1/4-750.

The small-angle X-ray scattering (SAXS) pattern for the representative Ni/MC-1/2-550 shows three well-resolved diffraction peaks at q values of 0.211, 0.327 and 0.437 $Å^{-1}$ with a ratio of 1: $3^{1/2}$: 2 (figure S6), associating with 10, 11 and 20 reflections of 2D hexagonal symmetry with the p6m space group [20].

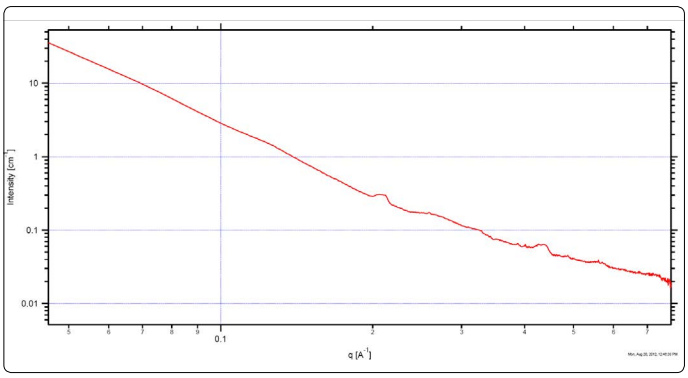

Figure S6. SAXS pattern of Ni/MC-1/2-550.

TEM images of Ni/CTS-1/2-550 shows highly dispersed spherical nanoparticles with average size centered at 34.7 nm (Figure 2a,d). However, Ni/CTS-1/2-750 and Ni/CTS-1/2-950 do not inherit the initial spherical shapes of Ni NPs, but rather exhibit irregularly congregated NPs with increased average diameter (Figure 2b,e,c,f). HRTEM images show clear lattice fringes throughout the whole particle, and the fringes in (111) direction is 0.203 nm, irrespective of the pyrolysis temperature (Figure 2g,h). Correspondingly, the electron microdiffraction of single Ni NP demonstrates the fm-3m symmetrical structure figure 2i and the selected area electron diffraction (SAED) pattern for Ni/MC-1/2-550 exhibits diffraction rings with fcc polycrystalline figure 2j, confirming XRD findings.

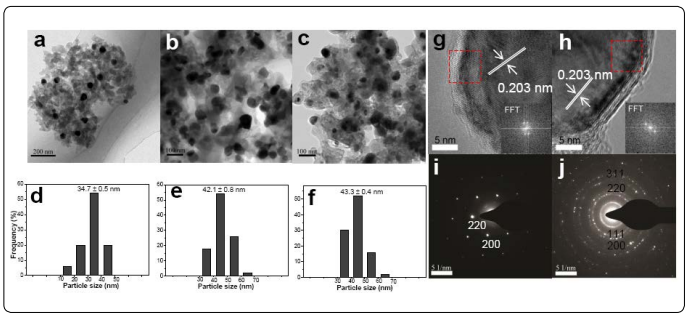

Figure 2. TEM images and the corresponding particle size distributions of (a,d) Ni/MC-1/2-550, (b,e) Ni/MC-1/2-750 and (c,f) Ni/MC-1/2-950, and HRTEM, electron microdiffraction and selected area electron diffraction images of (g,i,j) Ni/MC-1/2-550 and (h) Ni/MC-1/2-750.

Textual properties

N_2 adsorption reveals an IV type isotherm with a sharp inflection step at P/P_0 ranging from 0.25 to 0.35 (Figue 3A), characteristic of mesoporous materials [21,22].

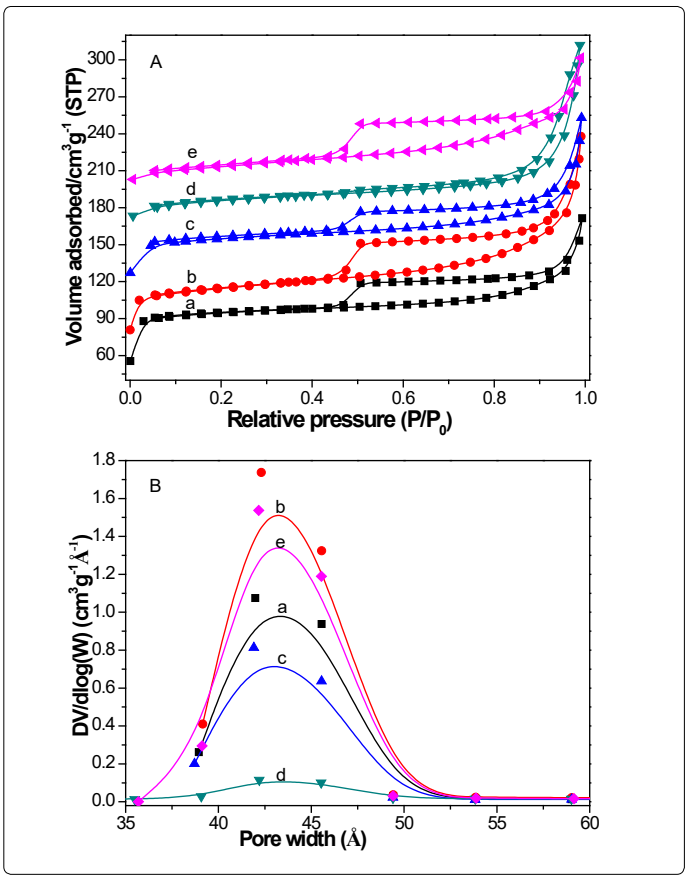

Figure 3. (A) N_2 adsorption/desorption isotherms and (B) BJH pore size distributions of (a) Ni/MC-1/1-750, (b) Ni/MC-1/2-750, (c) Ni/MC-1/4-750, (d) Ni/MC-1/2-550 and (e) Ni/MC-1/2-950. (b), (c), (d) and (e) were offset for 40, 70, 110 and 170 $cm^3 g^{-1}$, respectively.

Except for Ni/MC-1/2-550, all Ni/MC-x-t samples show H_2-type along with H_3-type hysteresis loops in higher P/P_0 region according to the IUPAC classification, corresponding to structural bottle-ink pores combined with piled mesopores [22]. The surface areas and pore volumes of the Ni/MC-x-t series vary with the Ni/CTS molar ratio and pyrolysis temperature. As shown in (Table 1).

Table 1. Characteristics of Ni/MC-x-t series, BET surface area, S_{BET} ($m^2 g^{-1}$); micropore surface area, S_{micro} ($m^2 g^{-1}$); pore volume, V_p ($cm^3 g^{-1}$); micropore volume, V_{micro} ($cm^3 g^{-1}$); pore diameter, D_p (nm) and CHN analysis (wt%)

Materials	S_{BET} ($m^2 g^{-1}$)[a]	S_{micro} ($m^2 g^{-1}$)	V_p ($cm^3 g^{-1}$)[b]	V_{micro} ($cm^3 g^{-1}$)[c]	D_p (nm)[d]	CHN analysis (wt%)		
						C	H	N
Ni/MC-1/1-750	301.9	246.4	0.237	0.115	4.32	-	-	-
Ni/MC-1/2-750	243.0	177.9	0.225	0.078	4.27	63.7	0.57	1.92
Ni/MC-1/4-750	271.7	214.1	0.245	0.099	4.26	-	-	-
Ni/MC-1/2-550	252.8	188.6	0.249	0.081	4.33	49.3	1.04	5.54
Ni/MC-1/2-950	143.1	93.9	0.174	0.038	4.28	75.5	0.40	0.86

[a]The BET surface area was obtained from the adsorption branches in the relative pressure range of 0.05-0.20.

[b]The single point adsorption total pore volume was taken at the relative pressure of 0.99.

[c] Micropore volume was calculated by *t-plot* method.

[d]The pore size distribution was calculated from the desorption branches by the Barret-Joyner-Halenda (BJH) method.

BET surface areas and pore volumes decrease first from 271.7 $m^2 g^{-1}$ and 0.245 $m^3 g^{-1}$ for Ni/MC-1/4-750 to 243.0 $m^2 g^{-1}$

and 0.225 $m^3 g^{-1}$ for Ni/MC-1/2-750, respectively, and then increase to 301.9 $m^2 g^{-1}$ and 0.237 $m^3 g^{-1}$ for Ni/MC-1/1750. On the other hand, they show a decrease trend when elevating pyrolysis temperature from 550 to 950 °C for Ni/MC-1/2-t series, and the N content also decreases correspondingly owing to the more amine fragments being removed. Whereas, all Ni/MC-x-t samples show pore sizes around 4.30 nm figure 3B, probably that Ni NPs are mainly embedded into the carbonaceous framework.

FT-IR studies

As illustrated in figure S7, the precursor composite Ni/CTS-P-1/2 shows C-H stretches at 2970 and 2926 cm^{-1} ascribed to PPO and PEO moieties for surfactant P123, and characteristic phenyl and byridyl vibrations between 1600 and 1300 cm^{-1}, suggesting that CTS-HQ has been incorporated into P123-directed superamolecular aggregates [23-24]. However, these peaks disappear after the simultaneous P123 removal and CTS carbonization upon being pyrolyzed at 750 and 950 °C, though there is some residue when pyrolyzed at 550 °C.

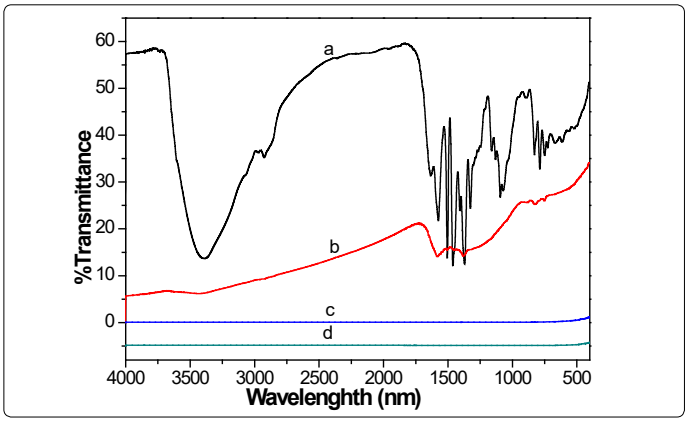

Figure S7. FT-IR spectra of (a) Ni/CTS-P-1/2, (b) Ni/MC-1/2-550, (c) Ni/MC-1/2-750 and (d) Ni/MC-1/2-950.

X-ray absorption fine structure

Nickel specific X-ray absorption fine structure (XAFS) were carried out to explore the local structure ranged from 1 to 3 Å, since the local structural information may closely correlate with catalytic properties. As illustrated in figure 4A, compared to nickel acetate and Ni/CTS-P-1/2, Ni/MC-x-t samples exhibit the decreased white line intensity along with the newly present pre-edge peak at ca. 8320 eV, suggesting the Ni(+2) species are mostly reduced [25-26], though Ni NPs carry some positive charges because of a slightly positive shifted edge position as compared to Ni reference [27]. In the corresponding k space, Ni/MC-x-t series show clear oscillations at a higher k region of k > 8 $Å^{-1}$ as compared to nickel acetate and Ni/CTS-P-1/2 figure S8, indicating the dominance of high Z backscatters, which would be Ni in our system. Consistently, Ni/MC-x-t series show prominent Ni-Ni contributions centered at 2.2 Å, different from the dominated Ni-O/C pairs at ca. 1.6 Å for Ni(+2)-containing samples (Figure 4B).

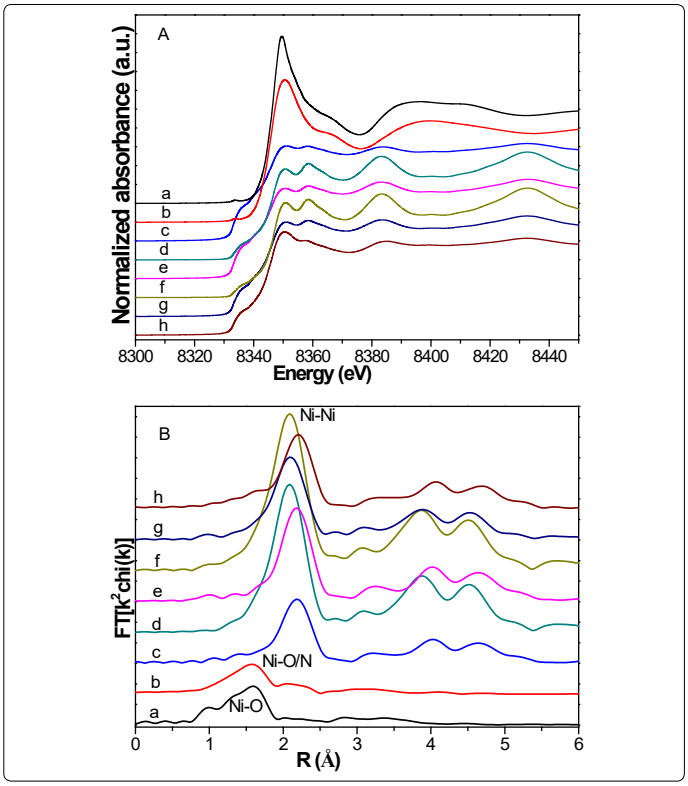

Figure 4. Ni K-edge XANES and the corresponding FT-EXAFS spectra for (a) $Ni(CH_3COO)_2 \cdot 4H_2O$, (b) Ni/CTS-P-1/2, (c) Ni/MC-1/2-550, (d) Ni/MC-1/2-750, (e) Ni/MC-1/2-950, (f) Ni/MC-1/1-750, (g) Ni/MC-1/4-750 and (h) Ni foil

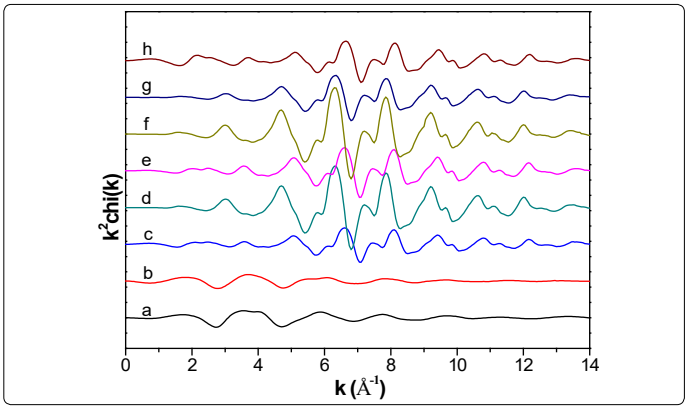

Figure S8. Normalized EXAFS (Ni K-edge scan) plotted as k^2*chi(k) *vs* k for (a) $Ni(CH_3COO)_2 \cdot 4H_2O$, (b) Ni/CTS-P-1/2, (c) Ni/MC-1/2-550, (d) Ni/MC-1/2-750, (e) Ni/MC-1/2-950, (f) Ni/MC-1/1-750, (g) Ni/MC-1/4-750 and (h) Ni foil.

On the other hand, Ni-Ni peak intensity varies with the Ni/CTS molar ratio and pyrolysis temperature. The peak intensity is proportional to the coordination number. As illustrated in (Table 2),

Table 2. Best fit parameters obtained from the analysis of the Ni K-edge EXAFS spectra[a]

Materials	Shell	Fitting range Δr [Å]	CN	R [Å]	σ^2 [$Å^2$]	ΔE_0 [eV]	S_0^2	R-factor (%)
Ni/MC-1/2-550	Ni-Ni	1.19-2.92	5.5	2.48	0.00575	4.876	1.378	0.061
Ni/MC-1/2-750	Ni-Ni	1.01-2.85	7.3	2.48	0.00750	-9.138	4.321	0.010
Ni/MC-1/2-950	Ni-Ni	1.15-2.66	8.1	2.48	0.00582	4.970	2.016	0.003
Ni/MC-1/1-750	Ni-Ni	1.18-2.61	11.2	2.48	0.00808	-9.240	4.979	0.004
Ni/MC-1/4-750	Ni-Ni	1.16-2.58	6.2	2.49	0.00629	-9.121	2.065	0.011
Ni foil	Ni-Ni	-	12.0	2.48	-	-	-	-

[a] CN = coordination number, R = bond distance, σ^2 = Debye-Waller factor, ΔE_0 = inner potential correction and S_0^2 = amplitude reduction factor.

The coordination number (curve-fitted values) increases from 5.5 for Ni/MC-1/2-550 figure s9 to 8.1 for Ni/MC-1/2-950, indicating larger Ni NPs formed at higher pyrolysis temperature. Increasing Ni/CTS molar ratio also brings a raise in coordination number from 6.2 for Ni/MC-1/4-750 to 11.2 for Ni/MC-1/1-750. However, All Ni/MC-x-t samples have smaller coordination numbers than that of Ni foil (CN = 12), suggesting that the Ni NPs are coordinatively unsaturated.

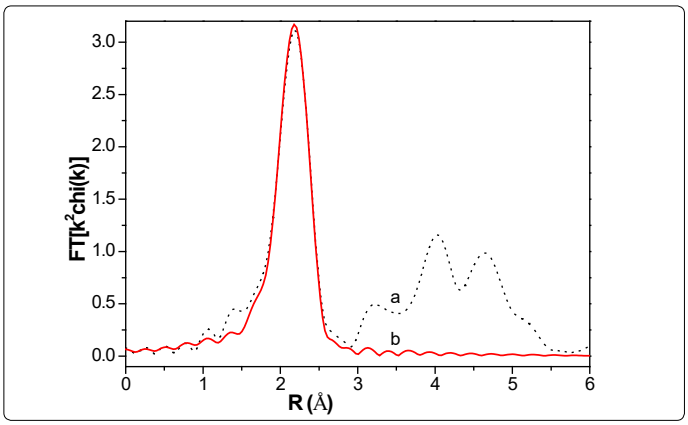

Figure S9. Curve fitting for Ni/MC-1/2-550 (red line).

Catalytic properties

We chose sorbitol hydrogenolysis as a probe reaction to investigate the catalytic performances of Ni/MC-x-t series, as such reaction is a promising green process to produce important commodity chemicals from biomass instead of petroleum table 3, summarizes the catalytic results for the hydrogenolysis of sorbitol over various samples.

Table 3. Sorbitol conversion and product selectivity over various samples

Entry	Materials	Metal content (mmolg^{-1})	Sorbi-tolcon-version[a] (%)	Product selectivity[b] (%)					TON[d]
				1,2-PG	EG	Sum	MeOH and EtOH	gaseous products[c]	
1	MC	0	3.0	-	-	-	-	-	-
2	Ni/MC-1/4-550	2.474	75.6	15.9	12.6	28.5	47.8	23.7	26.3
3	Ni/MC-1/2-550	3.940	86.0	12.7	12.4	25.1	46.9	28.0	18.8
4	Ni/MC-1/1-550	5.532	94.0	11.2	9.1	20.3	32.1	47.6	14.6
5	Ni/MC-1/4-750	2.215	37.3	14.5	11.0	25.5	39.5	35.0	14.5
6	Ni/MC-1/2-750	4.259	70.6	11.6	9.4	21.0	36.2	42.8	14.3
7	Ni/MC-1/1-750	4.400	54.4	9.0	6.4	15.4	30.8	53.8	10.6
8	Ni/MC-1/4-950	2.215	37.7	9.9	7.7	17.6	37.6	44.8	14.6
9	Ni/MC-1/2-950	3.578	41.6	9.5	7.5	17.0	35.0	48.0	10.0
10	Ni/MC-1/1-950	5.111	43.7	14.3	10.1	24.4	29.5	46.1	7.4
11	Ni/MC-1/2-550 (2nd)	-	99.9	2.7	4.9	7.6	52.3	40.1	-
12	Ni/MC-1/2-550 (3rd)	-	96.0	3.0	6.9	9.9	55.9	34.2	-
13	Ni/MC-1/2-550 (4th)	-	98.5	1.0	1.6	2.6	48.8	48.6	-
14	Ni/MC-1/2-550 (5th)	-	98.3	1.3	1.8	3.1	45.7	51.2	-
15	Ni/C-1/2-550[e]	-	9.6	3.7	7.5	11.2	36.9	51.9	-

[a]Reaction conditions: sorbitol 0.5g, catalyst 0.05 g, CaO0.5 g, H_2O 5.0 ml, H_2pressure 6 MPa, temperature 220°C and duration 4 h.

[b]1,2-PG: 1,2-propylene glycol and EG: ethylene glycol.

[c]including CH_4, H_2, C_2H_6 and C_3H_8, etc.

[d]TON: (turnover number) moles of sorbitol converted per mole nickel.

[e]Prepared by pyrolysis of chitosan-nickel metal coordination polymer in the absence of P123.

It is clear that all Ni/MC-x-t catalysts show relatively higher sorbitol conversion (> 35.0%) than MC (3.0%), substantiating that the active sites are Ni NPs, not mesoporous support. However, Ni/C-1/2-550, comparatively prepared *via* pyrolysis of chitosan-nickel coordination polymer (Supporting Information), is lack of uniform mesopore distribution figure S10, and exhibits insignificant activity (9.6%), suggesting the mesoporous arrays also play a role. In this study, the nanopores for Ni/MC-x-t series are much larger (around 4.30 nm) than the molecular dimensions of sorbitol (0.67 nm × 0.53 nm × 0.29 nm), facilitating mass transportation.

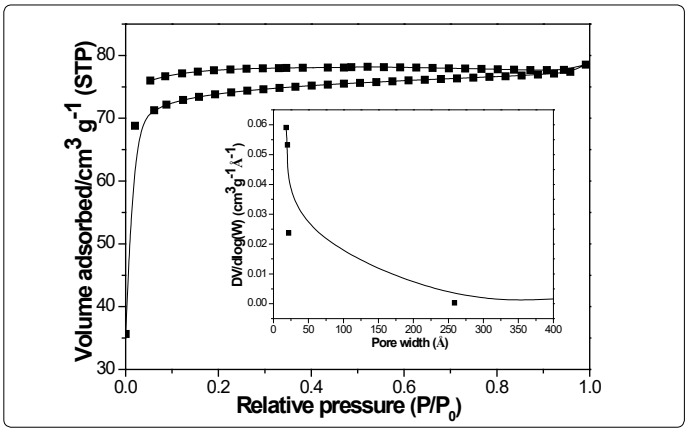

Figure S10. N_2 adsorption/desorption isotherm and BJH pore size distribution (inset) of Ni/C-1/2-550.

Ni/CTS molar ratio and pyrolysis temperature affect the catalytic properties of Ni/MC-x-t series significantly. As illustrated in table 3, except for Ni/MC-1/2-750, the sorbitol conversion improves with the increase of Ni content over different Ni/MC-x-550, Ni/MC-x-750 and Ni/MC-x-950 samples, respectively. For example, Ni/MC-1/4-550 shows 75.6% conversion of sorbitol, and Ni/MC-1/1-550 exhibits improved conversion of 94.0% (Table 3, entries 2-4), probably proportionate to the amount of available active Ni species in these catalysts. On the other hand, lower pyrolysis temperature is more beneficial to sorbitol conversion, since Ni/MC-x-550 series are more active than Ni/MC-x-750 and Ni/MC-x-950 series, verified by larger TON values. For nickel catalyzed sorbitol hydrogenolysis, the product distribution is complex because of various possible splitting styles of sorbitol under reaction conditions (Scheme S1). In this study, glycerol (GL), erythritol (C4-ol) and xylitol (C5-ol) are not detected. The selectivity to 1,2-PG is larger than to EG for all Ni/MC-x-t catalysts, though the total selectivity to 1,2-PG and EG is no more than 30%. These data demonstrate that glycol and glycerol are not the final products but the intermediate products which can undergo further hydrogenolysis to produce smaller species like EtOH, MeOH and gaseous products. The overall mass balances were always worse than 80%, suggesting large conversion of sorbitol or intermediates into gaseous products [9]. From this point of view, the lower selectivity to 1,2-PG and EG can be understandable since the unsaturated intermediates produced *via* retro-aldol condensation cannot be hydrogenated over Ni catalysts, and thus they have to undergo some base-catalyzed by-reactions [20]. The Ni catalysts pyrolyzed at higher temperatures destroyed their selectivity to 1,2-PG and EG, maybe related to

the large and irregular conglomeration of NPs. Among nickel based mesoporous carbons, Ni/MC-1/2-550 exhibits superior activity and total selectivity to 1,2-PG and EG, ascribed to the uniform spherical morphology and more coordinatively unsaturated nature.

The recoverability and stability of catalysts are further investigated. table 3 (entries 11-14) shows the recycling results of the representative Ni/MC-1/2-550. It is clear that Ni/MC-1/2-550 shows good recoverability without significant loss of activity even being recycled four times, though the total selectivity to 1,2-PG and EG decreases slightly. The Ni content in the filtrate was checked after the 1st use by ICP-AES, showing insignificant loss of 0.08% of Ni species. It is acknowledged that sorbitol can form chelate complexes with nickel in aqueous solution, and thus most Ni-containing catalysts cannot be recycled [11]. Ce-promoted Ni catalyst shows enhanced stability [8], while the pure Ni nanocatalyst in this study can be recycled well, probably ascribed to the enhanced interaction between Ni NPs and support created simultaneously during pyrolysis.

Conclusion

A series of nickel based mesoporous carbons have been successfully fabricated via pyrolysis of chitosan-nickel superamolecular aggregates with different Ni/CTS molar ratios at different temperatures. P123-directed self-assembly of CTS-HQ and nickel acetate guarantees the even dispersion of Ni species in the precursor composite Ni/CTS-P-x, rendering the homogeneously distributed Ni NPs inside the mesoporous carbonaceous framework after pyrolysis, and verified by various characterization techniques, such as high-energy X-ray diffraction, small-angle X-ray scattering, TEM, N_2 adsorption/desorption and X-ray absorption fine structure. Tuning of Ni/CTS molar ratio and pyrolysis temperature results in Ni/MC-1/2-550 catalyst with superior activity, total selectivity to 1,2-PG and EG recycling stability for the hydrogenolysis of sorbitol. This is probably related to the uniform spherical Ni nanoparticles on mesoporous carbons, as well as its more coordinatively unsaturated nature.

Acknowledgements

We thank the proposals (GUP28010 and GUP31195) given by Advanced Photon Source of Office of Science, U.S. Department of Energy under Contract DE-AC02-06CH11357.

References

1. Chheda JN, Huber GW, Dumesic JA. Liquid-phase catalytic processing of biomass-derived oxygenated hydrocarbons to fuels and chemicals. *Angew Chem Int Ed Engl*. 2007; 46(38): 7164-7183. doi: 10.1002/anie.200604274

2. Ruppert AM, Weinberg K, Palkovits R. Hydrogenolysis goes bio: from carbohydrates and sugar alcohols to platform chemicals. *Angew Chem Int Ed Engl*. 2012; 51(11): 2564-2601. doi: 10.1002/anie.201105125

3. Huber GW, Iborra S, Corma A. Synthesis of Transportation Fuels from Biomass: Chemistry, Catalysts, and Engineering. *Chem. Rev*. 2006; 106(9): 4044-4098. doi: 10.1021/cr068360d

4. Zhou CH, Xia X, Lin CX, Tong DX, Beltramini J. Catalytic conversion of lignocellulosic biomass to fine chemicals and fuels. *Chem. Soc. Rev*. 2011; 40(11): 5588-5617. doi: 10.1039/c1cs15124j

5. Yu WQ, Xu J, Ma H, et al. A remarkable enhancement of catalytic activity for KBH_4 treating the carbothermal reduced Ni/AC catalyst in glycerol hydrogenolysis. *Catal. Commun*. 2010; 11(5): 493-497. doi : 10.1016/j.catcom.2009.12.009

6. Banu M, Venuvanalingam P, Shanmugam R, Viswanathan B, Sivasanker S. Sorbitol hydrogenolysis over Ni, Pt and Ru supported on NaY. *Top Catal*. 2012; 55(11-13): 897-907. doi : 10.1007/s11244-012-9864-5

7. Hoffer BW, Prochazka R. US 2010/0019191 A1, 2010.

8. Ye LM, Duan XP, Lin HQ, Yuan YZ. Improved performance of magnetically recoverable Ce-promoted Ni/Al2O3 catalysts for aqueous-phase hydrogenolysis of sorbitol to glycols. *Catal. Today*. 2012; 183(1): 65-71. doi: 10.1016/j.cattod.2011.08.006

9. Banu M, Sivasanker S, Sankaranarayanan TM, Venuvanalingam P. Hydrogenolysis of sorbitol over Ni and Pt loaded on NaY. *Catal. Commun*. 2011; 12(7): 673-677. doi: 10.1016/j.catcom.2010.12.026

10. Wang XC, Meng LQ, Wu F, Jiang YJ, Wang L, Mu XD. Efficient conversion of microcrystalline cellulose to 1,2-alkanediols over supported Ni catalysts. *Green Chem*. 2012; 14(3): 758-765. doi: 10.1039/C2GC15946E

11. Schimpf S, Louis C, Claus P. Ni/SiO_2 catalysts prepared with ethylenediamine nickel precursors: Influence of the pretreatment on the catalytic properties in glucose hydrogenation. *Appl. Catal. A: Gen*. 2007; 318: 45-53. doi: 10.1016/j.apcata.2006.10.034

12. van Ryneveld E, Mahomed AS, van Heerden PS, Green MJ, Friedrich HB. A catalytic route to lower alcohols from glycerolusing Ni-supported catalysts. *Green Chem*. 2011; 13(7): 1819-1827. doi: 10.1039/C0GC00839G

13. Song Q, Wang F, Xu J. Hydrogenolysis of lignosulfonate into phenols over heterogeneous nickel catalysts. *Chem. Commun*. 2012; 48(56): 7019-7021. doi: 10.1039/C2CC31414B

14. Lee J, Kim J, Hyeon T. Recent Progress in the Synthesis of Porous Carbon Materials. Adv. Mater. 2006; 18(16): 2073-2094. doi: 10.1002/adma.200501576

15. Pang JF, Wang AQ, Zheng MY, et al. Catalytic conversion of cellulose to hexitols with mesoporous carbon supported Ni-based bimetallic catalysts. *Green Chem*. 2012; 14(3): 614-617. doi: 10.1039/C2GC16364K

16. Li ZL, Liu JH, Huang ZW, Yang Y, Xia CG, Li FW. One-Pot Synthesis of Pd Nanoparticle Catalysts Supported on N-Doped Carbon and Application in the Domino Carbonylation. *ACS Catal*. 2013; 3(5): 839-845. doi: 10.1021/cs400077r

17. Ma SQ, Goenaga GA, Call AV, Liu DJ. Cobalt Imidazolate Framework as Precursor for Oxygen Reduction Reaction Electrocatalysts. *Chem. Eur. J*. 2011; 17(7): 2063-2067. doi: 10.1002/chem.201003080

18. Kumar MNVR. A Review of Chitin and Chitosan Applications. *React. Funct. Polym*. 2000; 46(1): 1-27.

19. Guskos N, Typek J, Padlyak BV, et al. In situ synthesis, morphology and magnetic properties of poly(ether–ester) multiblock copolymer/carbon-covered nickel nanosystems. *J. Non-Cryst. Solids*. 2010; 356(37-40): 1893-1901. doi: 10.1016/j.jnoncrysol.2010.07.014

20. Zhao L, Zhou JH, Chen H, Zhang MG, Sui ZJ, Zhou XG. Carbon nanofibers supported Ru catalyst for sorbitol hydrogenolysis to glycols: Effect of calcination. *Korean J. Chem. Eng*. 2010; 27(5): 1412-1418. doi: 10.1007/s11814-010-0257-9

21. Corma A. From Microporous to Mesoporous Molecular Sieve Materials and Their Use in Catalysis. *Chem. Rev*. 1997; 97(6): 2373-2420. doi: 10.1021/cr960406n

22. Robles-Dutenhefner PA, Rocha KAD, Sousa EMD, Gusevskaya EV. Cobalt-catalyzed oxidation of terpenes: Co-MCM-41 as an efficient shape-selective heterogeneous catalyst for aerobic oxidation of isolongifolene under solvent-free conditions. *J. Catal*. 2009; 265(1): 72-79. doi: 10.1016/j.jcat.2009.04.012

23. Gallo JMR, Pastore HO, Schuchardt U. Silylation of [Nb]-MCM-41 as an efficient tool to improve epoxidation activity and selectivity. *J. Catal*. 2006; 243(1): 57-63. doi: 10.1016/j.jcat.2006.07.002

24. Maurya MR, Sikarwar S. Oxidation of phenol and hydroquinone catalysed by copper(II) and oxovanadium(IV) complexes of N,N′-bis(salicyledene) diethylenetriamine (H_2saldien) covalently bonded to chloromethylated polystyrene. *J. Mol. Catal. A: Chem*. 2007; 263(1-2): 175-185. doi: 10.1016/j.molcata.2006.08.038

25. Sarma LS, Chen CH, Kumar SMS, et al. Formation of Pt-Ru Nanoparticles in Ethylene Glycol Solution: An in Situ X-ray Absorption Spectroscopy Study. *Langmuir*. 2007; 23(10): 5802-5809. doi: 10.1021/la0637418

26. Daniel OM, DeLaRiva A, Kunkes EL, Datye AK, Dumesic JA, Davis RJ. X-ray Absorption Spectroscopy of Bimetallic Pt-Re Catalysts for Hydrogenolysis of Glycerol to Propanediols. *ChemCatChem*. 2010; 2(9): 1107-1114. doi: 10.1002/cctc.201000093

27. Qiao BT, Wang AQ, Yang XF, et al. Single-atom catalysis of CO oxidation using Pt1/FeOx. *Nat. Chem*. 2011; 3(8): 634-641. doi: 10.1038/nchem.1095